Detection, 2014, 2, 1-6
Published Online January 2014 (http://www.scirp.org/journal/detection)
http://dx.doi.org/10.4236/detection.2014.21001

Scientific Research

Theoretical D^* Optimization of N^+-p $Pb_{1-x}Sn_xSe$ Long-Wavelength (8 - 11 μm) Photovoltaic Detector at 77 K

Binbin Weng, Jijun Qiu, Lihua Zhao, Caleb Chang, Zhisheng Shi

The School of Electrical and Computer Engineering, University of Oklahoma, Norman, USA.
Email: binbinweng@ou.edu

Received December 1st, 2013; revised January 2nd, 2014; accepted January 10th, 2014

ABSTRACT

In this work, the study of the influences of lifetime, doping concentration and absorption layer thickness to resistant-area product (R_0A) and quantum efficiency of $Pb_{1-x}Sn_xSe$ photovoltaic detector are presented. Three fundamental current mechanisms including diffusion, generation-recombination, and tunneling models are considered. Using optimal doping concentration and absorption layer thickness parameters, the calculated detectivity (D^*) of $Pb_{1-x}Sn_xSe$ photovoltaic detector is over 10^{12} cm $Hz^{1/2}$/W.

KEYWORDS

$Pb_{1-x}Sn_xSe$; Lifetime; Resistant-Area Product; Quantum Efficiency; Detectivity

1. Introduction

Mid- and long-infrared light detection in the atmosphere windows (3 - 5 um and 8 - 14 um) has widespread military and civilian applications. There is an increasing demand to have a large format and long wave infrared imaging system. Existing technologies are mainly based on semiconductor photo-detectors [1]. HgCdTe (MCT) is currently the premier material of interest for mid- and long-wave IR focal plane array (FPA) applications. The best MCT material is produced by MBE on CdZnTe substrates. However, these substrates are costly, brittle, and of small size. For large format FPA applications, many major players are transferring the growth and processes of MCT to alternative substrates, mainly Silicon. The transfer is complicated by a 19% lattice mismatch and nearly 100% thermal mismatch. The results are a mid- to high- 10^6 cm^{-2} dislocation density which has deleterious effect on the final FPA. Other alternatives such as III-V materials are facing similar challenges pertaining to the large-sized substrate.

IV-VI semiconductors such as $Pb_{1-x}Sn_xSe$ offer high sensitivity similar to MCT [2]. Until the end of the 1970s, both materials were intensively developed with comparable effort for mid-IR detector applications. MCT became predominantly the material of choice mainly because the permittivity of IV-VI materials is lower than that of MCT, which leads to slow RC response time. At that time, the concerns pertaining to the single-element detector were legitimate. However, this argument does not apply to staring imaging systems that contain a large number of sensors. The large dielectric constant, which is more than 10 times that of MCT, becomes advantageous because coulomb scattering by ionized impurities is strongly suppressed. Consequently, the electric field caused by such defects is shielded within a very short distance. Therefore, IV-VI Pb-salt materials are much more tolerant to defects in comparison to MCT. Due to this effect, Pb-salt materials could have approximately one order of magnitude higher performance than MCT for the same dislocation density [3].

It has been demonstrated that high quality IV-VI semiconductors can be grown on Si substrate. The mismatch of the thermal expansion coefficient was well addressed by a thin CaF_2 buffer layer. Dislocation gliding on (111)-

oriented substrate reduces the threading dislocation density caused by lattice and thermal expansion mismatch [4]. Recently, we have developed a growth method for IV-IV materials on Si substrate that reduces the etch pit density down to 10^5 cm^{-2} [5]. These advantages make IV-VI materials promising candidates for large-format long wave infrared FPA [6].

In this paper, we present a theoretical investigation for IV-VI $Pb_{1-x}Sn_xSe$ in the long wavelength spectral range (8 - 11 μm). The influences of different generation-recombination mechanisms to the carrier lifetime are discussed. The resistant-area product (R_0A) is divided into three parts for the discussion: diffusion, recombination in junction area, and tunneling. The optimized doping concentration and layer thickness are calculated. The optimized detectivity is over 10^{12} cm Hz$^{1/2}$/W.

2. Theory

2.1. Carrier Lifetime

The carrier generation-recombination mechanisms in detector devices are distinguished as band to band Auger's, radiative and Shockley-Read-Hall's (SRH) generation-recombination mechanisms. Among them, SRH's mechanism is determined by the material quality. Auger's and radiative mechanisms are determined by energy band structures. Therefore, those two are fundamentally limiting factors for the overall generation-recombination processes. In this paper, we consider only Auger's and radiative mechanisms to exam the PbSnSe material system. More realistic simulation can be performed by considering SRH's mechanism for a given material quality.

For the radiative process, in case of the Boltzmann statistics, the carrier lifetime is determined by [7]:

$$\tau_r^{-1} = 2B\left(N_A^2/4 + n_i^2\right)^{1/2},$$

where

$$B = \frac{2n_r q^2\left(2p_t^2 + p_l^2\right)Eg^4}{9\pi^3\hbar^4 c^3\left(p_t p_l n_i\right)^2} F(\beta),$$

N_A is the acceptor concentration which is assumed to be equal to the major carrier concentration in *p*-type layer, and n_i is the intrinsic carrier concentration. The function $F(\beta)$ is defined as:

$$F(\beta) = 1/\beta^{3/2}\int_0^\infty \sqrt{t + t^2/\beta}\left(3 + 8t/\beta + 8t^2/\beta^2\right) \times \exp\left(-\beta - 2t\right)dt$$

in which $\beta = Eg/(k_B T)$, n_r is the refractive index, p_t and p_l are the momentum matrix elements, Eg is the band gap energy. Based on the experimental data, it is reasonable to assume that the doping concentration $N_A \gg n_i$, consequently, the corresponding carrier lifetime leads to $\tau_r = 1/(N_A B)$. For the carrier lifetime depending on Auger's process, the relationship is given by $\tau_A = \left[C_A\left(N_A^2 + 2n_i^2\right)\right]^{-1}$ [8]. In the case of $N_A \gg n_i$, the simplified Auger's carrier lifetime equation is derived as $\tau_A = \left(C_A N_A^2\right)^{-1}$. The Auger's recombination coefficient C_A is defined as [9]:

$$C_A = \frac{3q^4(2\pi)^{5/2}(k_B T)^{1/2} Eg^{-7/2}h^3}{\left(16\pi\varepsilon_0\varepsilon_\infty\right)^2 m_l^{*1/2} m_t^{*3/2}} \times \exp\left[-\frac{Eg}{2k_B T}\left(\frac{m_l^*}{m_t^*}\right)^{-1}\right],$$

where m_l^* and m_t^* are the longitudinal and transverse effective masses.

2.2. Resistant Area Product (R_0A)

For the R_0A calculation, we made following assumptions in our model. Firstly, the photodiode in this model is N$^+$-p hetero-structure (the capital letter means the material has larger band gap energy, symbol "+" denotes high doping concentration). The lightly doped p-type layer is sandwiched between the substrate silicon and highly doped, wider band gap N$^+$ layer. The wider band gap N$^+$ layer has smaller absorbance and lower intrinsic carrier concentration. In such a structure, the *p*-type absorption layer determines both dark current I_d and photocurrent I_p of the diode. Secondly, the carrier lifetime is only determined by Auger and radiative mechanisms. Thirdly, we assume the carrier mobility at 77 K is a constant value of 2 × 10^4 cm^2/Vs. Fourthly, the dark current is determined by diffusion-drift, generation-recombination and tunneling mechanisms. Finally, we assume that the front side surface is well passivated. Due to the back-side illumination mode (light incident through substrate side) and the wider-gap layer, influence of surface recombination on the top surface can be eliminated. The schematic band diagram of epitaxial N$^+$-p $Pb_{1-x}Sn_xSe$ hetero-junction photodiode is presented in **Figure 1**.

The R_0A product is contributed by diffusion-drift (R_0A_{DD}), generation-recombination (R_0A_{GR}) and tunneling (R_0A_T) processes: $(R_0A)^{-1} = (R_0A_{DD})^{-1} + (R_0A_{GR})^{-1} + (R_0A_T)^{-1}$. The R_0A product derived from diffusion current is given by

$$R_0A_{DD} = \frac{k_B T L_n}{q^2 D_n n_p}\coth\left(w_p/L_n\right)$$ [10],

where D_n is the diffusion coefficient, L_n is the electron diffusion length which is equal to $\sqrt{D_n\tau_n}$, w_p is the thickness of *p* layer, n_p is the minority concentration in *p* layer. The generation-recombination R_0A_{GR} determined by the depletion area current is expressed by the equation

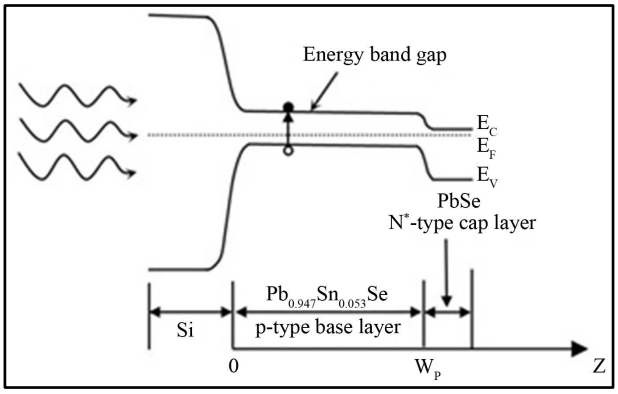

Figure 1. Schematic energy band diagrams of epitaxial N+-p $Pb_{1-x}Sn_xSe$ hetero-structure.

$$R_0A_{GR} = \frac{\left(E_g N_A\right)^{1/2}\tau_0}{qn_i(2\varepsilon_0\varepsilon_s)^{1/2}} \quad [11],$$

where ε_s is the static dielectric constant. We assume that the lifetime in junction and neutral area is the same. The contribution to R_0A by the tunneling mechanism is given by

$$R_0A_T = \pi^3\hbar^2\left(\varepsilon_s\varepsilon_0\right)^{1/2}\times \exp\left[\frac{\pi\left(m_x^*\varepsilon_s\varepsilon_0\right)^{1/2}Eg}{2^{3/2}q\hbar N_A^{1/2}}\right]\Bigg/\left(q^3\sqrt{2N_Am_y^*m_z^*/m_x^*}\right) \quad [12],$$

where m_x^*, m_y^*, and m_z^* are the orientation dependent effective mass components. For IV-VI materials, they are given in Table 1.

2.3. Quantum Efficiency

The reflectivity of radiation is a limiting factor for quantum efficiency. IV-VI group materials have very large dielectric constants. As a result, for the frontside illumination mode, the reflection loss can be more than 50%, for the backside illumination mode, the loss just decreases down to 30% due to the lower dielectric constant of the substrate Si. However, antireflection coating can be used to increase transimission close to unity. In this work, we assume the light incidence is 100% transmission.

In the hetero-junction structure, Rosenfeld etc. used one dimensional model to derive the net quantum efficiency. Its formula is slightly modified in this work and shown as follows [14]:

$$\eta = \frac{G_2\left(w_p\right)+G_1\left(w_p\right)}{\cosh\left(L_n^{-1}w_p\right)},$$

where

$$G_{1,2}\left(z\right) = \frac{1}{\varphi_0}\int_0^z G_L\left(z\right)\exp\left(\pm L_n^{-1}u\right)du,$$

Table 1. Orientation dependent effective mass [13].

Orientation	m_x^*	m_y^*	m_z^*	Valley
[111]	m_t^*	m_t^*	m_l^*	$[111]$
	m_t^*	$\frac{8m_l^*+m_t^*}{9}$	$\frac{9m_l^*m_t^*}{8m_l^*+m_t^*}$	$\left[1\bar{1}\bar{1}\right]$
	$\frac{2m_l^*+m_t^*}{3}$	$\frac{\left(8m_l^*+m_t^*\right)m_t^*}{6m_l^*+3m_t^*}$	$\frac{9m_l^*m_t^*}{8m_l^*+m_t^*}$	$\left[\bar{1}1\bar{1}\right]$, $\left[\bar{1}\bar{1}1\right]$
[110]	m_t^*	$\frac{m_l^*+2m_t^*}{3}$	$\frac{3m_l^*m_t^*}{m_l^*+2m_t^*}$	$[111]$, $\left[11\bar{1}\right]$
	$\frac{2m_l^*+m_t^*}{3}$	$\frac{3m_l^*m_t^*}{2m_l^*+m_t^*}$	m_t^*	$\left[\bar{1}1\bar{1}\right]$, $\left[\bar{1}\bar{1}1\right]$
[100]	$\frac{m_l^*+2m_t^*}{3}$	$\frac{2m_l^*+m_t^*}{3}$	$\frac{3m_l^*m_t^*}{2m_l^*+m_t^*}$	$[111]$, $\left[11\bar{1}\right]$, $[111]$, $\left[11\bar{1}\right]$

where the monochromatic backside illumination generation rate $G_L(z)$ is defined as

$$G_L = \alpha\left(z\right)\varphi_0\exp\left[-\int_0^z\alpha\left(u\right)du\right],$$

in which φ_0 is the photon flux at the edge of the absorption layer (z = 0) and $\alpha(z)$ is the absorption coefficient which is dependent on Sn composition. It is given by the two band model relation

$$\alpha = \frac{\sqrt{2}}{5}\times\frac{q^2m_t\left(2p_t^2+p_l^2\right)}{\pi n_r c\varepsilon_0\hbar^4Eg}\times\frac{2\left(\hbar\omega\right)^2+Eg^2}{3\left(\hbar\omega\right)^2} \times\left[m_l\left(\hbar\omega-Eg\right)\left(\frac{\hbar\omega}{Eg}+1\right)\right]^{1/2} \quad [15],$$

in which ω stands for the angle frequency of the incident light.

The quantum efficiency described above is associated with the monochromatic photon flux. However, the detectors are normally exposed to a wide spectral range flux as described by Plank's radiation law. Consequently, the weighted average of the quantum efficiency can be given by

$$\eta_{AVE} = \frac{\int_{\lambda_1}^{\lambda_2}\eta\left(\lambda\right)n\left(\lambda\right)d\lambda}{\int_{\lambda_1}^{\lambda_2}n\left(\lambda\right)d\lambda},$$

where $n(\lambda)$ is the spectral radiant photon emittance of the target.

2.4. Detectivity

The detectivity is the most important figure of merit for detectors. The Johnson-Nyquist noise dependent detec-

tivity is given by $D^* = \frac{q\eta\lambda}{hc}\sqrt{\frac{R_0A}{4k_BT}}$. From this formula, it is denoted that D^* is associated with both resistant area product R_0A and quantum efficiency η. Shot noise dependent detectivity is not discussed in our model.

3. Results and Discussions

3.1. Optimization of Doping Concentration

The parameters for the simulation are listed in Table 2. As can be seen, all of the parameters except mobility and ε_s are dependent on Sn composition and the temperature. In terms of this condition, the simulated results should be convincible in $Pb_{1-x}Sn_xSe$ system. The Sn compositions of 0.053 and 0 are used for p-type $Pb_{0.947}Sn_{0.053}Se$ layer and N^+PbSe layer, respectively.

Figure 2 shows Auger's lifetime (solid dot), radiative lifetime (solid square) and the total lifetime (solid line) with acceptor concentration in p layer of $Pb_{0.947}Sn_{0.053}Se$. While N_A is larger than 1×10^{17} cm^{-3}, Auger's mechanism dominates the material lifetime. The lifetime is less than 10 ns when the doping concentration is 2×10^{17} cm^{-3}. When N_A is lower than 1×10^{17} cm^{-3}, lifetime influenced by the radiative mechanism is increasing more slowly than the Auger's one. The lifetime is over 100ns when concentration is 3×10^{16} cm^{-3}. This is because Auger's lifetime is proportional to N_A^{-2} and radiative lifetime is proportional to N_A^{-1}. In all, total lifetime decreases rapidly with the increase of N_A.

Figure 3 shows the R_0A for different doping concentrations N_A at 77 K. The thickness of p layer is 16 μm. Three mechanisms are taken into consideration. The resistant area product R_0A caused by the tunneling process is proportional to exponential N_A^{-1}, as a result, R_0A drops dramatically as N_A is over 1×10^{17} cm^{-3}. Overall, R_0A decreases with the increase of N_A, and the value varies slightly when N_A is under 1×10^{17} cm^{-3}.

Therefore, both lifetime and R_0A increase as the acceptor concentration N_A decreases. Since the typical N_A for $Pn_{1-x}Sn_xSe$ is between 1×10^{16} cm^{-3} and 1×10^{17} cm^{-3} at 77 K, we use N_A of 3×10^{16} cm^{-3}. The corresponding lifetime is approximately 100 ns. The diffusion length L_n is 36.4 μm. In this case, the diffusion length is twice as long as the absorption thickness. Thus, all carriers generated in this layer will be collected.

3.2. Optimization of the Thickness of Absorption Layer

The quantum efficiency is sensitive to the thickness of the absorption layer. Based on the discussion above, we use a lifetime of 100 ns and N_A of 3×10^{16} cm^{-3}, and the energy band gap of 0.115 eV. (Corresponding wavelength is 11 μm). Figure 4 shows the relationship between

Table 2. Physics properties of $Pb_{1-x}Sn_xSe$ [11], [16], [17].

Parameters	$Pb_{1-x}Sn_xSe$
$Eg(x,T)$	$0.125-1.021x+\left(4\times10^{-4}+2.56\times10^{-7}\times T^2\right)$
m_{te}^*	$\left[20.7\times Eg(0,0)/Eg(x,T)+4.3\right]^{-1}\times m_0$
m_{le}^*	$\left[11.4\times Eg(0,0)/Eg(x,T)+2.9\right]^{-1}\times m_0$
m_{th}^*	$\left[20.7\times Eg(0,0)/Eg(x,T)+8.7\right]^{-1}\times m_0$
m_{lh}^*	$\left[11.4\times Eg(0,0)/Eg(x,T)+3.3\right]^{-1}\times m_0$
ε_∞	$(107/Eg)^{1/2}$
n_0	$(107/Eg)^{1/4}$
ε_s	227 at 77 K
μ_n	2×10^4 cm^2/Vs

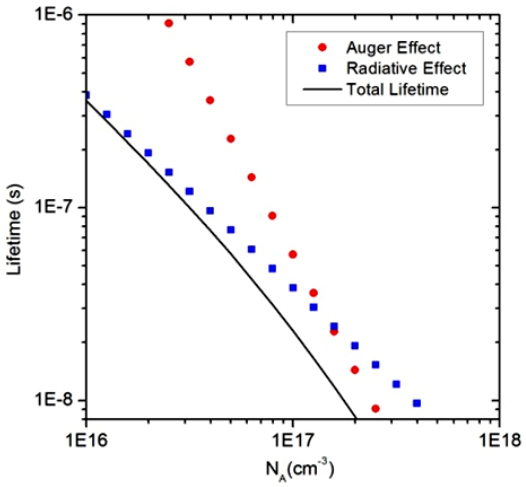

Figure 2. Lifetime versus acceptor concentrations at 77 K.

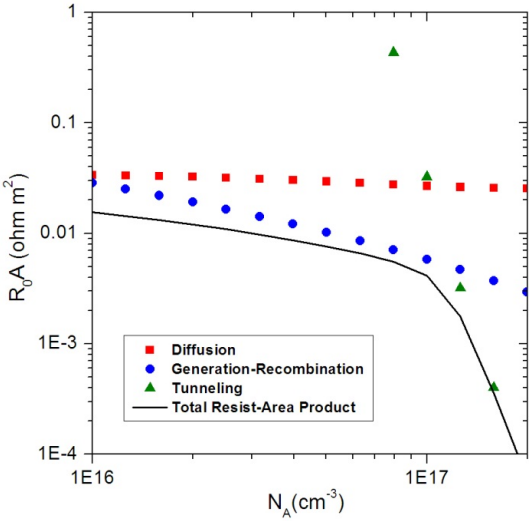

Figure 3. The resistant area product R_0A versus acceptor concentration N_A at 77 K.

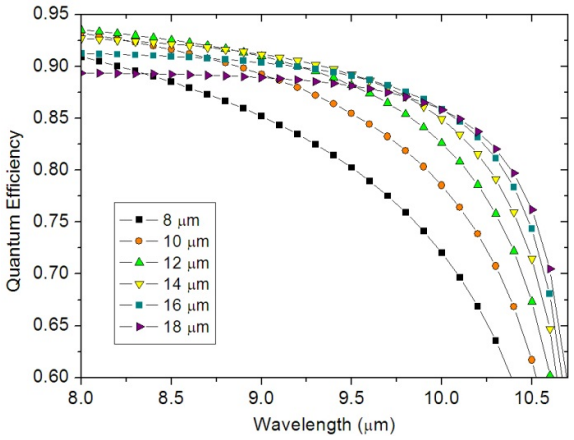

Figure 4. Quantum efficiency with different thicknesses in long wavelength range at 77 K.

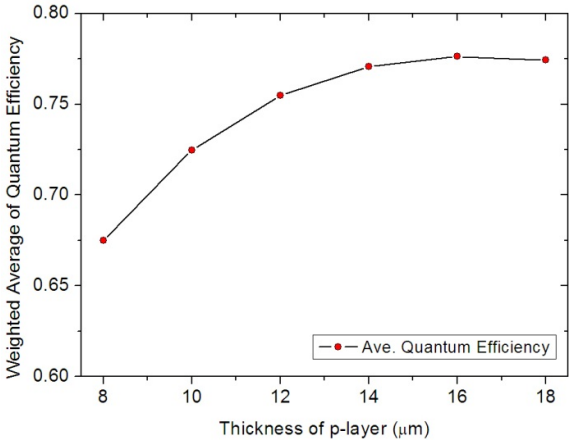

Figure 5. The weighted average of quantum efficiency versus the thickness of player at 77 K.

quantum efficiency and absorption thickness in the long wavelength spectral range 8 to 11 μm. In this figure, quantum efficiencies decrease as incident wavelength increases. As can been seen, 12 μm thickness gives the highest value of about 95% at 8 μm.

We apply weighted average of quantum efficiency to define the optimal thickness with the best performance. The background radiation temperature is at 300 K. The simulation result is given in **Figure 5**. It denotes average quantum efficiency rising rapidly from 8 μm to 14 μm. And around 16 μm thickness, the quantum efficiency value reaches the peak.

3.3. Detectivity

With the calculated quantum efficiency and lifetime value. **Figure 6** shows the simulated D^* for different $Pb_{1-x}Sn_xSe$ *p*-type layer thickness at 77 K. For thickness between 10 to 18 μm, D^* value is over 10^{12} cm $Hz^{1/2}$/W.

To our knowledge, the highest reported theoretical D^* for HgCdTe N^+-p photodiode in long wavelength spectral range (8 - 11 μm) is 9×10^{10} cm $Hz^{1/2}$/W at 77 K [18]. We would like to point out that their simulation included the surface recombination process with a surface recombination velocity (SRV) of 10^4 cm/s. When we consider surface recombination using the same SRV the R_0A changed slightly from 41 to 40 ohm·cm^2. Since quantum efficiency depends weakly on SRV our simulated D^* value remains almost the same. This D^* value of $Pb_{1-x}Sn_xSe$ is more than one order of magnitude larger than the simulated D^* of MCT's in reference [18].

4. Conclusion

The one dimensional $Pb_{1-x}Sn_xSe$ photovoltaic diode simulation model has been discussed in this work. We calculated the lifetime, R_0A, absorption, quantum efficiency and detectivity for structure N^+-p heterojunction on Si

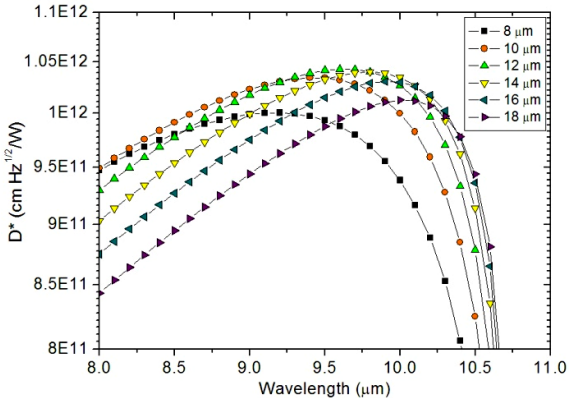

Figure 6. Detectivity D^* versus absorption thickness in 8 - 11 μm spectral range at 77K.

substrate. The optimized D^* value obtained is over 10^{12} cm $Hz^{1/2}$/W. This result indicates a great potential for PbSnSe detector with superior detectivity to be fabricated.

Acknowledgements

We acknowledge financial supports from the DoD AFOSR under Grant No. FA9550-12-1-0451, DoD ARO Grant No. W911NF-07-1-0587, and Oklahoma OCAST program under Grant No. AR112-18 and No. AR132-003.

REFERENCES

[1] A. Rogalski, "Infrared Detectors: Status and Trends," *Progress in Quantum Electronics*, Vol. 27, No. 2-3, 2003, pp. 59-210. http://dx.doi.org/10.1016/S0079-6727(02)00024-1

[2] A. Rogalski, "Analysis of the R_0A Product in n^+-p $Hg_{1-x}Cd_xTe$ Photodiodes," *Infrared Physics*, Vol. 28, No. 3, 1988, pp. 139-153. http://dx.doi.org/10.1016/0020-0891(88)90002-4

[3] S. Elizondo, F. Zhao, J. Kar, J. Ma, J. Smart, D. Li, S. Mukherjee and Z. Shi, "Dielectric Charge Screening of

Dislocations and Ionized Impurities in PbSe and MCT," *Journal of Electronic Materials*, Vol. 37, No. 9, 2008, pp. 1411-1414. http://dx.doi.org/10.1007/s11664-008-0418-3

[4] P. Muller, H. Zogg, A. Fach, J. John, C. Paglino, A. N. Tiwari and M. Krejci, "Reduction of Threading Dislocation Densities in Heavily Lattice Mismatched PbSe on Si(111) by Glide," *Physical Review Letters*, Vol. 78, 1997, pp. 3007-3010. http://dx.doi.org/10.1103/PhysRevLett.78.3007

[5] B. Weng, F. Zhao, J. Ma, G. Yu, J. Xu and Z. Shi, "Elimination of Threading Dislocations in As-Grown PbSe Film on Patterned Si(111) Substrate Using Molecular Beam Epitaxy," *Applied Physics Letters*, Vol. 96, 2010, Article ID: 251911. http://dx.doi.org/10.1063/1.3457863

[6] H. Zogg, A. Fach, C. Maissen, J. Masek and S. Blunier, "Photovoltaic Lead-Chalcogenide on Silicon Infrared Sensor Arrays," *Optical Engineering*, Vol. 33, No. 5, 1994, pp. 1440-1449. http://dx.doi.org/10.1117/12.165808

[7] O. Ziep, D. Genzow, M. Mocker and K. H. Herrmann, "Nonradiative and Radiative Recombination in lead Chalcogenides," *Physica Status Solidi* (*b*), Vol. 99, No. 1, 1980, pp. 129-138. http://dx.doi.org/10.1002/pssb.2220990111

[8] A. Rogalski and W. Larkowski, "Comparison of Photodiodes for the 3-5.5 um and 8-14 um Spectral Regions," *Electron Technology*, Vol. 18, 1985, pp. 55-69.

[9] P. R. Emtage, "Auger Recombination and Junction Resistance in Lead-Tin Telluride," *Journal of Applied Physics*, Vol. 47, 1976, pp. 2565-2568. http://dx.doi.org/10.1063/1.322975

[10] D. Rosenfeld, V. Garber and G. Bahir, "The Effects of Built-in Electric Field on the Performance of Compositionally Graded P-on-n HgCdTeHeterojunction Photodiodes," *Journal of Applied Physics*, Vol. 77, 1995, pp. 925-933. http://dx.doi.org/10.1063/1.359020

[11] A. Rogalski and W. Kaszuba, "Photovoltaic Detectors $Pb_{1-x}Sn_xSe$ ($0<x<0.12$). Minority Carrier Lifetimes. Resistance-Area Product," *Infrared Physics*, Vol. 21, No. 5, 1980, pp. 251-259. http://dx.doi.org/10.1016/0020-0891(81)90030-0

[12] W. W. Anderson, "Tunnel Contribution to $Hg_{1-x}Cd_xTe$ and $Pb_{1-x}Sn_xTe$ p-n Junction Diode Characteristics," *Infrared Physics*, Vol. 20, No. 6, 1980, pp. 353-361. http://dx.doi.org/10.1016/0020-0891(80)90052-4

[13] T. N. Xu, "Optical Properties of IV-VI Semiconductor Low-Dimensional structures," Ph.D. Dissertation, Department of Physics, Zhejiang University, Zhejiang, 2008.

[14] D. Rosenfeld, V. Garber and G. Bahir, "The Effect of Built-in Electric Field on the Performance of Compositionally Graded P-on-n HgCdTe Heterojunction Photodiodes," *Journal of Applied Physics*, Vol. 77, 1994, pp. 925-933. http://dx.doi.org/10.1063/1.359020

[15] O. Ziep and D. Genzow, "Calculation of the Interband Absorption in Lead Chalcogenides Using a Multiband Model," *Physica Status Solidi* (*b*), Vol. 96, No. 1, 1979, pp. 359-368. http://dx.doi.org/10.1002/pssb.2220960138

[16] H. Perier, "Recent Advances in Lead-Chalcogenide Diode Lasers," *Applied Physics*, Vol. 20, No. 3, 1979, pp. 189-206. http://dx.doi.org/10.1007/BF00886018

[17] R. Dalven, "A Review of the Semiconductor Properties of PbTe, PbSe, PbS and PbO," *Infrared Physics*, Vol. 9, No. 4, 1969, pp. 141-184. http://dx.doi.org/10.1016/0020-0891(69)90022-0

[18] V. Dhar and R. Ashokan, "A Model for Quantum Efficiency and Detectivity of n^+p and n^+n^-p $Hg_{1-x}Cd_xTe$ Photodiodes," *Semiconductor Science and Technology*, Vol. 12, No. 5, 1997, pp. 580-588. http://dx.doi.org/10.1088/0268-1242/12/5/011